IET Renewable Power Generation

Special Issue Call for Papers

Be Seen. Be Cited.
Submit your work to a new IET special issue

Connect with researchers and experts in your field and share knowledge.

Be part of the latest research trends, faster.

Read more

The Institution of Engineering and Technology

Received: 17 January 2021 | Revised: 31 March 2021 | Accepted: 28 April 2021

IET Renewable Power Generation

DOI: 10.1049/rpg2.12204

The Institution of Engineering and Technology WILEY

ORIGINAL RESEARCH PAPER

Opening the air-chamber of an oscillating water column spar buoy wave energy converter to avoid parametric resonance

Josh Davidson[1] | João C. C. Henriques[2] | Rui P. F. Gomes[2] | Roberto Galeazzi[3]

[1] Department of Fluid Mechanics, Faculty of Mechanical Engineering Budapest University of Technology and Economics, Budapest, Hungary

[2] IDMEC, Instituto Superior Técnico, Universidade de Lisboa, Lisbon, Portugal

[3] Department of Electrical Engineering, Technical University of Denmark, Lyngby, Denmark

Correspondence
Department of Fluid Mechanics, Faculty of Mechanical Engineering Budapest University of Technology, and Economics, Hungary.
Email: davidson@ara.bme.hu

Funding information
Portuguese Foundation for Science and Technology, Grant/Award Number: UID/EMS/50022/2020; H2020 Marie Skłodowska–Curie Actions, Grant/Award Number: 867453

Abstract

The oscillating-water-column (OWC) spar-buoy is a type of wave energy converter that may exhibit undesirable large roll and pitch amplitudes caused by a dynamic instability induced by parametric resonance. The occurrence of this phenomenon not only reduces the power extraction but significantly increases the structural loads on the buoy, the turbine rotor and on the mooring system. The paper compares the parametric resonance behaviour of two configurations of an OWC spar-buoy using experimental data obtained in a wave flume at a scale of 1:100. The configurations investigated were: (1) closed and (2) fully open-air chamber. The experimental tests covered a wide range of regular and irregular waves, as well as in free decay experiments. Results showed that opening the air chamber reduces the coupling between the buoy and the OWC within, thus shifting the damped natural heave frequency of the system in comparison with the closed chamber configuration. This effect changes parametric resonance characteristics of the two configurations due to the coupling between roll/pitch and heave modes. Moreover, for specific wave frequencies, the occurrence of parametric resonance observed when the chamber is closed do not occur while the air chamber is fully open. These results suggest the possibility of controlling a pressure relief valve installed on top of the device to reduce parametric resonance whenever this dynamic instability is detected.

1 | INTRODUCTION

An oscillating water column (OWC) spar buoy, is a type of wave energy converter (WEC) that utilises the relative heave motion between an outer spar hull and an inner moon pool-like water column to drive the air, enclosed in a chamber above the OWC, through a turbine installed at the top of the buoy and connected to the atmosphere. Like many offshore spar structures [1–4], this device is prone to large amplitude pitch and roll motions, caused by parametric resonance, when the frequency of the waves is around twice the pitch/roll natural frequency, see Figure 1. Parametric resonance is a dynamic instability caused by the time-varying changes in the parameters of a system [5], which manifests in floating offshore structures, due to the wave-induced heave motion of the structure varying the metacentric height.

The occurrence of parametric resonance in the OWC spar buoy severely reduces the heave motion and thus energy capture. Besides, large-amplitude pitch/roll motions can lead to structural and safety issues. Therefore, parametric resonance is a critical problem to be addressed and mitigated in the design of this type of WECs.

1.1 | Parametric resonance in spar type WECs

The concept of resonance is well known in WEC research and development since maximum energy extraction is typically achieved when the WEC natural frequency matches the peak frequency of the input wave field. By comparison, parametric resonance has received very little attention, probably since it is an effect not found in conventional numerical models favoured in WEC research and analysis. In recent years there is a growing interest in modelling and controlling parametric resonance in WECs [6]. This trend is demonstrated by the increasing number

FIGURE 1 Several consecutive positions of an OWC spar buoy in parametric resonance along the time. Pictures were taken at the NAREC large scale wave flume, Blyth, UK

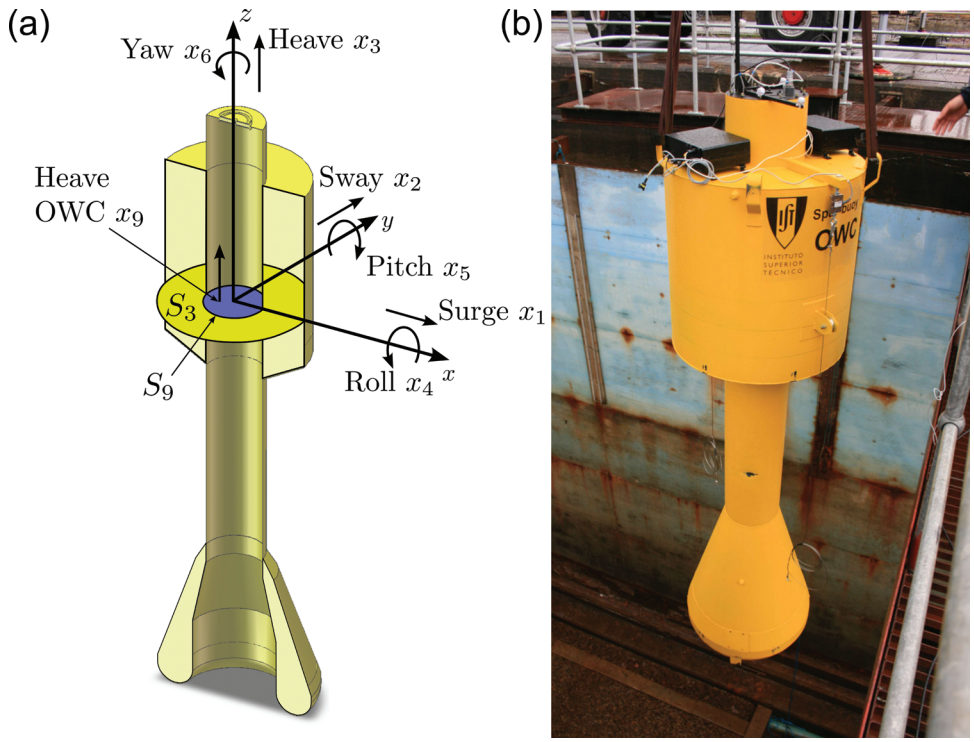

FIGURE 2 (a) Cut section view of an OWC spar buoy with indication of the fixed reference frame and oscillation modes. (b) The 1:16 scale OWC spar buoy model being installed at NAREC

of reported observations of parametric instabilities during wave tank experiments and the rise of nonlinear hydrodynamic models capable of simulating the occurrence of parametric resonance [7].

Spar type WECs tend to comprise two heaving bodies, extracting energy through their relative motion. Parametric instability in the pitch/roll degrees of freedom (DoFs) for these devices have been observed experimentally [8–10] and numerically [11, 12].

The OWC spar buoy also consists of two heaving bodies, the outer spar buoy and the inner OWC. The dynamic instability of the OWC spar buoy has been reported in several studies at various scales. It was first reported in [13] from a 1:120 scale testing of the device at the wave flume in Instituto Superior Técnico, Lisbon, Portugal. Further tests at the same scale are described in [14, 15], where the experimental results are compared against linear models, and large differences between the numerical and experimental results are observed for the pitch motion at twice the natural frequency due to parametric resonance. To test a passive control scheme to reduce the parametric resonance, more experiments were performed in the same wave flume at 1:100 scale in [16]. A 1:16 scale OWC spar buoy model was tested at the large scale wave flume of NAREC (Blyth, UK), where pitch and roll parametric resonance was observed and drastically reduced the power conversion performance [17], see Figures 1 and 2.

In addition to the experimental observations, the occurrence of parametric resonance in the OWC spar buoy has also been noted in several numerical studies. Ref. [12] used experimental data obtained by [16] for an OWC spar buoy to test the ability of a nonlinear hydrodynamic model to capture parametric resonance. The reported simulation results predicted the parametric resonance behaviour at the expected frequencies. The same modelling technique was then applied by [18] to the 1:16 scale OWC spar buoy tests described in [17] to investigate the effect of mooring lines parameters on the dynamic instability. This study concluded that the parametric roll response is found to have little dependence on the mooring lines configuration.

A procedure to identify the frequency and amplitude ranges in which parametric resonance will occur is included into the numerical optimisation method proposed by [19]. A penalty was added to the performance index of the configurations where parametric resonance was predicted.

A small number of studies have made initial attempts towards reducing parametrically excited pitch/roll motions in spar-type WECs. Most attempts use of passive mechanisms, such as fins or strakes, to increase the hydrodynamic damping in the pitch/roll DoFs. This approach has been shown to reduce the occurrence of parametric resonance in conventional spar platforms [2]. The use of strakes is numerically investigated in [9], after experimental testing of WaveBob-like two-body heaving point absorbers, revealed that power production is limited by the excessive pitch and roll motions when parametric resonance occurs. The simulation results confirm the ability of the strakes to reduce pitch and roll amplitudes, allowing increased WEC power output. The use of fins has been investigated for the stabilisation of the OWC spar buoy in [16].

The use of passive mechanisms may contribute to reducing parametric instability but it is unlikely to solve the problem unless the area of the fins/strakes is very large. The reason for this is easy to show. The damping moment M is proportional to $\dot{\theta}^2 A$, where $\dot{\theta}$ is the angular velocity and A is the fins/strakes area. Since the angular velocity has an order of magnitude of $\mathcal{O}[\dot{\theta}] = 0.1$ rad/s, the total area A needs to be large for the fins/strakes to have a significant impact on the damping of the pitch/roll motion. To properly mitigate the occurrence of parametric resonance, it is necessary to search for simple active methods.

1.2 | Active parametric resonance control

Villegas and van der Schaaf consider a two-body, self-reacting, heaving point absorber, the WaveBob [8]. Similar to the present case, parametric pitch/roll was detected in physical experiments, due to the detriment of the WEC performance. These authors proposed an active control system that acts on the WEC dynamics to mitigate the occurrence of parametric resonance. This control consists of acting on the PTO force between the two bodies. The PTO force couples the motion of the two-body system, influencing the resonant peaks in the frequency response of the heave, pitch and roll DoFs. The active control system proposed by Villages and van der Schaaf applies a notch filter, designed to eliminate any PTO forces at the frequencies for which parametric resonance occurs. Experimental results for a model scale device in a wave tank validate the effectiveness of this approach in ref. [8].

Further confidence in this strategy is provided by additional studies uncovered during the literature review for this paper. Ref. [20] experimentally tested a floating cylindrical OWC, considering five different orifice diameters in the OWC. Interestingly, extremely large amplitude roll motions, at twice the natural roll frequency, occur for one orifice diameter. For the other orifice diameters at this frequency, two had slightly larger than normal roll amplitudes, and the other two had normal roll amplitudes, compared to the amplitude trend of surrounding frequencies. This behaviour suggests that the occurrence of parametric resonance might be dependent on, and therefore controlled by, the PTO damping.

The experiments reported in ref. [21] aim to provide numerical validation for linear hydrodynamic models developed for a free-floating sloped WEC. This device has a fully submerged inclined open tube attached to a buoy. The tube contains a piston whose motion relative to the buoy-tube system drives the PTO mechanism. Thus energy extraction results from the relative motion between the large water mass inside the tube and the oscillating buoy-tube system. Experiments were performed with the tube open and blocked. Since the device is symmetric with respect to the incoming waves, the linear models cannot predict roll motion. However, significant roll motions are observed at specific frequencies due to parametric resonance. Interestingly, there is a shift in the frequencies for which parametric resonance occurred between the open and blocked tube configurations.

A number of similarities can be noticed between the WaveBob and the OWC spar buoy: they are both two-body spar buoy systems, where the heave motion of the bodies are coupled through the PTO. For OWC WECs, the PTO damping is determined by the turbine rotor diameter and, in the case of the Wells turbine, the rotational speed. The PTO damping for the case of the axial impulse and biradial turbines are independent or weakly dependent on the rotational speed. Increasing the turbine rotor size has the effect of increasing the PTO damping. For the Wells turbine, decreasing the rotational speed also increases the turbine damping. The opening of the air chamber is equivalent to reducing the PTO damping to zero and, therefore, has the same effect as the notch filter used to mitigate the occurrence of parametric resonance in the WaveBob [8].

1.3 | Objective and outline of paper

The paper compares the parametric resonance behaviour of two configurations of an OWC spar-buoy model using experimental data obtained in a wave flume. The experimental tests were conducted at a scale of 1:100 and the configurations investigated were: (1) closed and (2) fully open-air chamber. Hereinafter, these configurations are named ‘closed OWC” and “open OWC”. The tests contemplated a wide range of regular and irregular wave conditions. The results show that the two configurations exhibit different frequency responses. Thereby, this behaviour opens the possibility of detuning the frequency coupling (responsible for the existence of parametric resonance) by switching between the two configurations whenever parametric resonance is detected. This switching may be implemented through the operation of an air pressure relief valve installed in parallel with the PTO system, as an active control method to counteract the development of parametric resonance. The use of a relief valve was not considered for these experimental tests. The complexity of designing, building and controlling in real-time a small-scale relief valve installed in a buoy model was beyond the scope of this work.

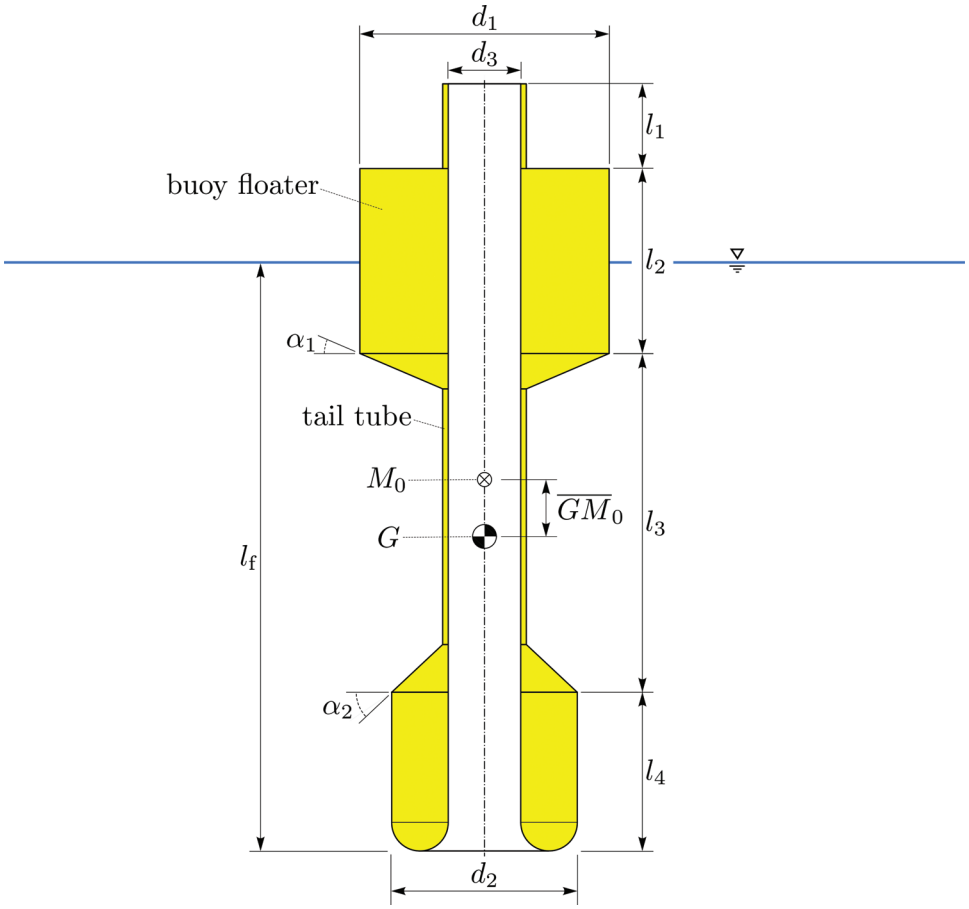

FIGURE 3 Cut-view of the OWC spar buoy model with the geometric dimensions

The paper is organised as follows. Section 2 reviews the theoretical background related to the occurrence of parametric resonance in the OWC spar buoy. Next, in Section 3, the paper reports on experiments performed to test the stated hypothesis, with a small-scale model OWC spar buoy in a wave flume. The results are presented in Section 4 and conclusions are drawn in Section 5.

2 | THEORETICAL BACKGROUND

The OWC spar buoy has two modes of parametric instability. The first mode is related to the heave motion, x_3, and appears when the buoy motion is such that the waterplane area has an abrupt change, as in the transition between the floater and the tail tube [22], see Figure 3.

$$m_{33}\ddot{x}_3 + \left(k + \Delta k\, f(t)\right) = 0, \tag{1}$$

where m_{33} is the buoy mass plus the added mass, k is the stiffness and Δk is the stiffness variation. The stiffness is defined by $k = \rho_w g A_w$ where ρ_w is the water density, g is the gravity acceleration, A_w is the water plane area of the floater. The stiffness variation is given by $\Delta k = \rho_w g \Delta A_w$ with ΔA_w the change of waterplane area between the buoy floater and the tail tube. Equation (1) can be written in the form

$$\ddot{x}_3 + \left(\omega_{n3}^2 + \frac{\Delta k}{m_{33}} f(t)\right) = 0, \tag{2}$$

where

$$\omega_{n3}^2 = \frac{k}{m_{33}}. \tag{3}$$

If we approximate the change from the floater waterplane area to the tail tube waterplane area by a step function, then $f(t)$ is a function defined by a square wave of period $T_{k3} = 2\pi/\omega_{k3}$, see Figure 4. An analytical solution of Equation (2) for the case when $f(t)$ is a square wave can be found in [23]. The solution shows an unstable behaviour when T_{k3} is equal to $\{T_{n3}/2, T_{n3}, 3T_{n3}/2, ...\}$. To the authors' knowledge, this type parametric instability was never reported in the literature for OWC spar buoys.

The second instability mode is similar but related to the pitch and roll motions [24]. For a cylindrical body, the equation of

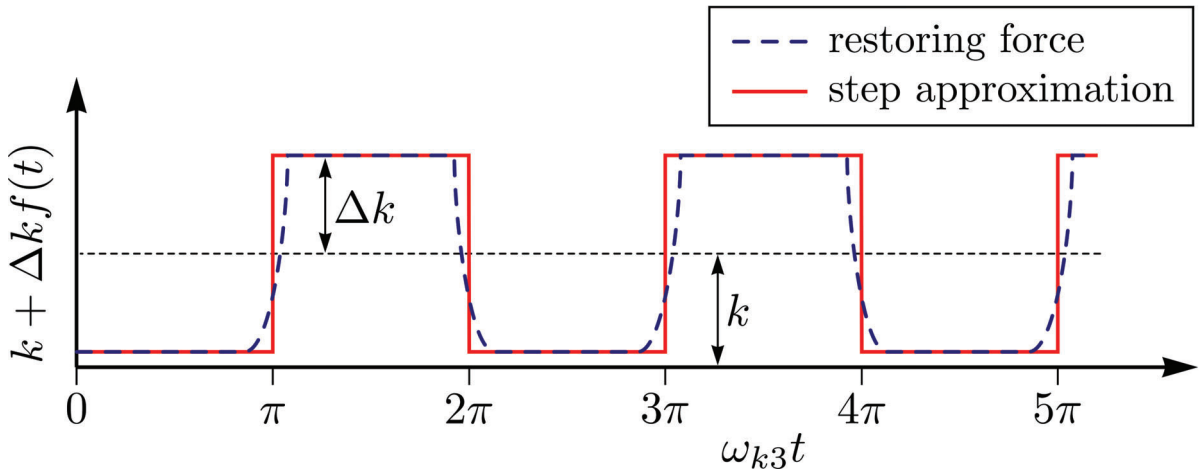

FIGURE 4 Variation of the restoring force in heave and step function approximation

motion for pitch, x_5, without excitation force is

$$I_{55}\ddot{x}_5 + b_{55}\dot{x}_5 + \rho_w g \nabla_0 \left(\overline{GM}_0 - \frac{1}{2}x_3\right)x_5 = 0, \qquad (4)$$

where I_{55} is the rotation moment of inertia plus added inertia, b_{55} is the linear damping coefficient, ∇_0 and $\overline{GM}_0$ are the displaced volume and metacentric height in calm water, see Figure 3.

To assess the effect of the heave motion on the dynamics of the pitch motion, let us write Equation (4) as a Mathieu type equation as in ref. [25]. For this, we assume that the heave displacement has a periodic variation $x_3 = \epsilon \cos(\omega_{k3} t)$, and apply a transformation of variables such that $\tau = \omega_{k3} t$, yielding

$$\frac{\mathrm{d}^2 x_5}{\mathrm{d}\tau^2} + \mu \frac{\mathrm{d}x_5}{\mathrm{d}\tau} + \left(\varpi^2 + \Lambda \cos\tau\right)x_5 = 0, \qquad (5)$$

where $\mu = b_{55}/(\omega I_{55})$, $\varpi = \omega_{n5}/\omega_{k3}$, and $\Lambda = \frac{1}{2}\varpi^2 \epsilon$.

The stability diagram of Equation (5) is plotted in Figure 5. This plot shows that the undamped system is unstable when $\varpi = 1/2$, i.e. when the frequency of the heave displacement is twice the natural frequency in pitch $\omega_{k3} = 2\omega_{n5}$. For small heave displacements ϵ, the damping prevents the appearance of the instability. Increasing the heave displacement ϵ, the system becomes unstable for a broad range of frequencies around $\omega_{k3} = 2\omega_{n5}$. For very large displacements, parametric resonance may even occur for frequencies around $\omega_{k3} = \omega_{n5}$.

Equation (5) shows that the open/closed OWC configurations may have an impact in the onset of the parametric resonance because of the change of the heave response amplitude ϵ and also on the natural frequency in heave ω_{k3}.

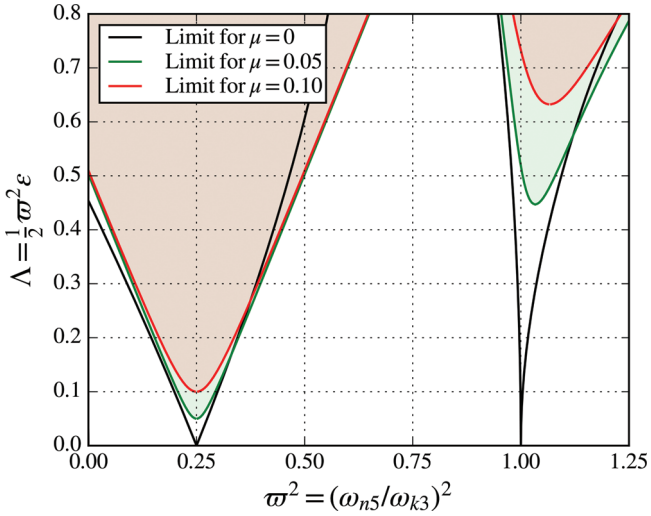

FIGURE 5 Stability diagram obtained from the Mathieu equation for different dimensionless damping values. The shaded areas denote unstable regions for the associated damping value. The horizontal dashed lines represent constant metacentric height parameter ε as a function of Δ

3 | EXPERIMENTS

The experiments were conducted at the wave flume in Instituto Superior Técnico, Lisbon, Portugal, which is 20 m long and 0.7 m wide. A water depth of 0.5 m was used. The flume is equipped with an HR Wallingford wave generation system with a piston-type wavemaker with active absorption of reflected waves and a constant-slope dissipative beach at the opposite end of the flume. The beach has a reflection coefficient below 10% for the range of wave frequencies and amplitudes used in the experiments. A schematic of the experimental setup is shown in Figure 6.

The experiments were performed using the same wave flume and OWC Spar Buoy model as in [16] but without dissipative fins on the model. The model geometry is based on the optimised geometry of the OWC spar buoy [26], with comparable diameter, draft and mass distribution, with the exception that the model's inner tube has a uniform cross-section. The full characteristics of the model are documented in [16]. The OWC spar buoy geometry is shown in Figure 3 while the experimental model is depicted in Figure 7.

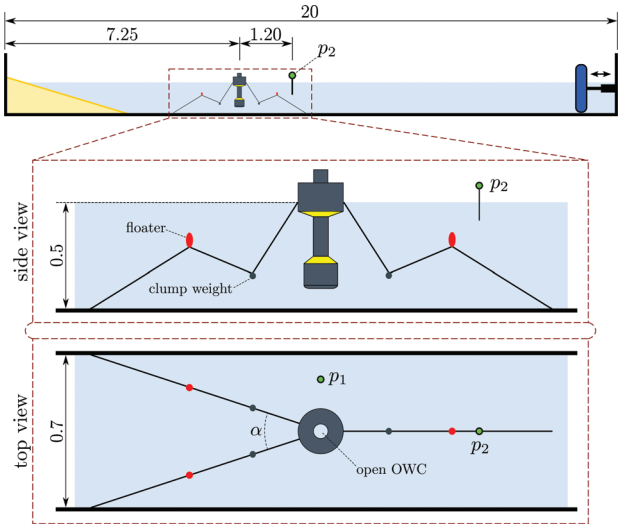

FIGURE 6 Schematic representation of the wave channel and of the OWC spar buoy model and its mooring system (not to scale). The wave probes are denoted by p_1 and p_2.

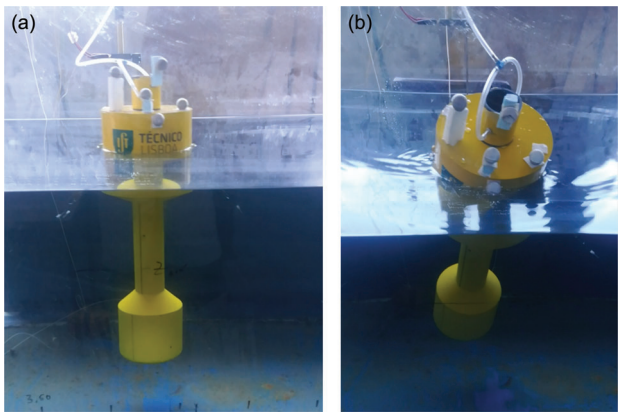

FIGURE 7 (a) Photo of the model OWC spar buoy, including the reflective markers used by the motion tracking system and the tube appendage for pressure measurement at its equilibrium position. (b) Photo taken during large amplitude parametric roll motion (here the opened top of the OWC can be seen)

Two different configurations of the model were used in the present experiments: (1) Closed OWC—where the top of the OWC chamber is air-tight, and (2) open OWC—where the top of the OWC chamber is fully open, see Figure 7(c). The general buoy dimensions are reported in Table 1.

The model was kept on station using a three-line, slack-mooring system, as illustrated in Figure 6, which was designed to reduce its influence on the heave motion dynamics. Each line is composed of three line-segments with a clump weight and a floater at the connection points. The fairleads are located at the free surface. Ideally, the three fairleads should be equally-spaced in the circumferential direction, with an angle of 120° between them. Since the channel dimensions do not allow it, the angle between the two lines on the leeward side of the OWC spar buoy was set to $\alpha = 29°$, see Figure 6. Although the same mooring configuration was applied as in [16], the mooring system was re-made using new lines, thus the clump weights, floaters and anchor weights may be located in slightly different positions. However, the study in ref. [18] showed the occurrence of PR in the OWC Spar Buoy is not sensitive to moderate changes in the parameters of the mooring system.

TABLE 1 General OWC spar buoy dimensions. The buoy geometry is described in Figure 3

Dimension	Value
d_1	0.160 m
d_2	0.120 m
d_3	0.050 m
l_1	0.549 m
l_2	0.121 m
l_3	0.217 m
l_4	0.102 m
l_f	0.375 m
α_1	22.2°
α_2	42.3°

The motion of the floating model was captured using a Qualisys 6-DoF motion tracking system, comprising a system of infrared cameras that captures the motion of reflective markers attached to the model (seen on the top of the model in Figure 7). Three infrared cameras (ProReflex) are positioned along the wave flume, with different view angles, at a distance of less than 2 m from the OWC spar buoy, enabling high resolution and accuracy for the Qualysis tracking system. The tolerance of the displacement measurement is estimated to be 0.3 mm. This value is based on the variation of the markers relative distances, when compared with the calibration baseline. This relates to a maximum error of approximately 1.3% for pitch/roll angles of 5°, 0.6% for angles of 10° and 0.4% for angles of 20°. Due to such high resolution and precision obtained by the close proximity of the infrared cameras, the associated error-bars and bounds of confidence in the measured results are of comparable thickness to the lines used to plot the graphs in Section 4.

The free surface elevation (FSE) was measured with resistive wave probes at two different locations within the wave flume, next to the model (p_1) and in front of the model (p_2), as displayed in Figure 6. Both body motion and FSE were sampled at 100 Hz. The pressure difference between the air chamber and the exterior atmosphere is measured, by a differential pressure sensor, connected to the model by a low weight tube appendage (seen on the top of the model in Figure 7). However, the pressure measurements were not used in the present work.

3.1 | Tests

Three sets of tests were performed in the wave flume: (1) free decay, (2) regular wave induced motion and (3) irregular waves induced motion experiments.

3.1.1 | Free decay

The free decay experiments were performed to determine the damped natural frequencies of the heave, pitch and roll motions. Although for an axisymmetric device, the pitch and roll DoFs should theoretically be identical, the mooring lines and the air tubes attached to the top of the buoy's air chamber introduce an asymmetry. Therefore, both pitch and roll DoFs were tested separately. The model was manually displaced from its equilibrium position and then released, with the resulting body motion being measured until the model comes to rest. The experiment was performed three times for each DoF, for both the open and closed OWC configurations. Results are shown in Section 4.1.

3.1.2 | Regular waves

To compare the frequency response of the open and closed OWC configurations, a series of experiments utilising regular waves with a range of frequencies were performed. A total of 27 different frequencies, spanning 0.4–1.3 Hz were tested, with a higher resolution around the frequencies where parametric resonance was observed. The target wave amplitude was set to 0.01 m, and each experiment lasts 120 s.

The waves were initially generated and measured in an empty tank (without the model in place). Next, the closed OWC model was placed in the tank and the resulting body motions were measured for the series of input waves. Then the top was removed from the model and the open OWC was tested. The results are presented in Section 4.2.

3.1.3 | Irregular waves

Finally, a series of irregular waves with varying peak frequency and significant wave height were tested. A total of 12 different sea states were generated, considering the combination of three peak frequencies (0.75, 1 and 1.25 Hz) and four significant wave heights (0.01, 0.02, 0.03 and 0.04 m), following a JONSWAP spectrum with spectral shape (Γ) equal to 1.0, typical of the North Atlantic coasts. Each sea state was generated twice, once for the closed OWC and another for the open OWC considering a duration of 900 s at model scale. The results are presented in Section 4.3.

4 | RESULTS

The results of the free decay tests are presented in Section 4.1 and the wave induced motion tests for the regular and irregular input waves are given in Sections 4.2 and 4.3, respectively.

4.1 | Free decay tests

The results of the free decay tests are plotted in Figure 8, showing the start of the recorded time series for the three heave, pitch

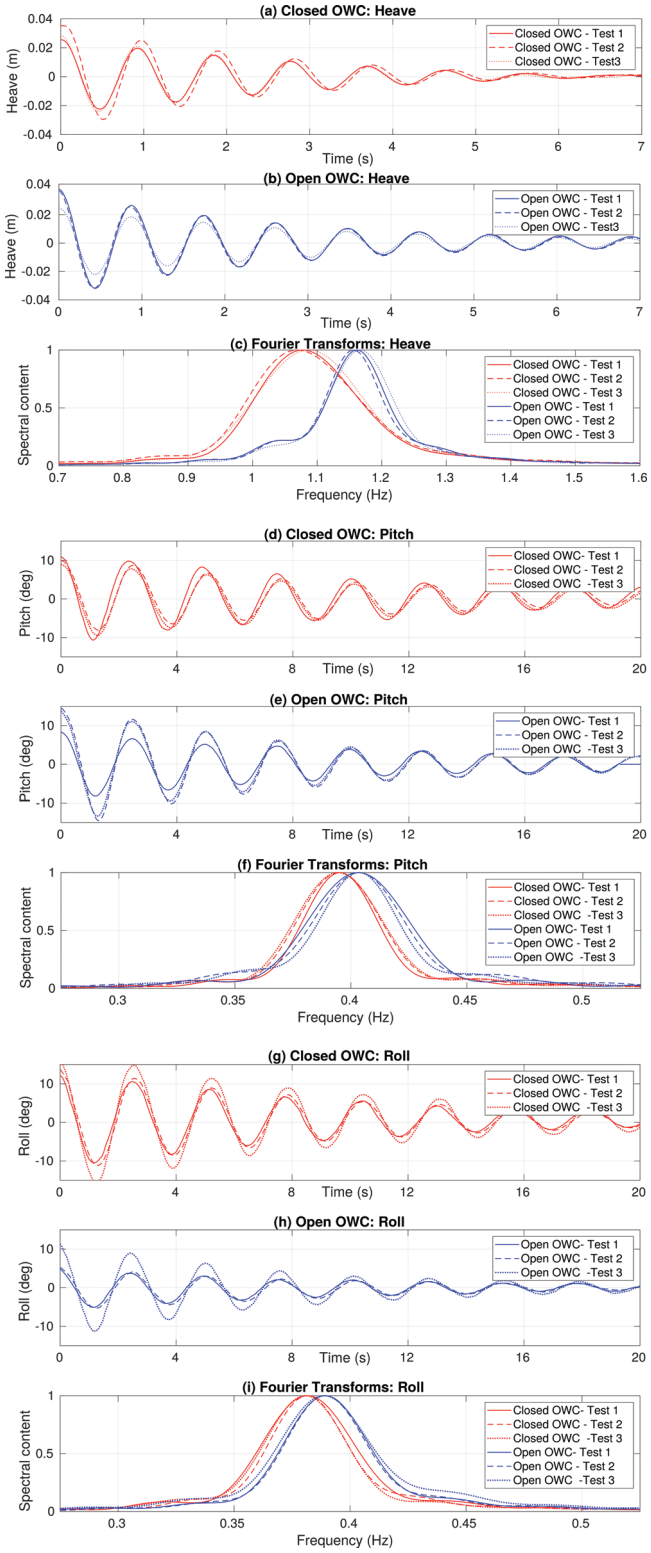

FIGURE 8 (a, b, d, e, g, h) The free decay time series and (c, f, i) their power spectra normalised against the peak value.

TABLE 2 Damped natural frequency for heave, pitch and roll DoFs, determined from the free decay experiments

		Test 1	Test 2	Test 3	Average
		[Hz]	[Hz]	[Hz]	[Hz]
Heave	Open	1.156	1.161	1.167	1.16
	Closed	1.070	1.078	1.087	1.08
Pitch	Open	0.403	0.404	0.404	0.40
	Closed	0.395	0.395	0.394	0.39
Roll	Open	0.389	0.389	0.389	0.39
	Closed	0.382	0.382	0.381	0.38

and roll experiments, for both the open and closed configurations. Additionally, the frequency spectrum for each of the time series is shown. To calculate the spectra, a fast Fourier transform (FFT) is used, and zero padding is added to the end of the free decay time signal to increase the resulting frequency resolution. The damped natural frequencies of the heave, pitch and roll DoFs are calculated using the peak of the spectra plotted in Figures 8(c, f, i), respectively, and confirmed by measuring the period between successive peaks in the time series. The results are recorded in Table 2.

Figure 8(a–c) show the heave free decay results. Table 2 shows that the damped natural pitch frequency is 0.39 Hz for the closed OWC and 0.40 Hz for the open OWC, and the damped natural roll frequency is 0.38 Hz for the closed OWC, and 0.39 Hz for the open OWC. Thus the change in damped natural frequency is only about 2.5%. The shift of the resonance to a lower frequency for the closed case, compared to the open case, agrees with the results found in [21].

A number of differences can be noted in the decay tests between the open OWC and the closed OWC configurations:

- The damped natural frequency of the two configurations is different.
  The peak frequencies of the free decay spectra show that the open OWC has higher damped natural frequencies for heave, pitch and roll than the closed OWC.
  In the case of the open OWC, the coupling between the buoy and the OWC inside is just the cross radiation terms and the water viscous stresses.
  The closed OWC shows an additional spring-like coupling between the buoy and the OWC inside due to the compressibility of the air in the chamber.
  Considering the added inertia in the closed OWC configuration from the OWC inside, a lower natural frequency is expected in comparison with the open OWC.
- For the heave motion, the open OWC has a second smaller frequency peak at 1.04 Hz.
  This is due to the dynamics of the water column, since two-body systems can have twin peaks in their frequency response.
  For the closed OWC, the motion of the water column and body are locked together, resulting in a single peak between the twin peaks of the open OWC.
  This type of behaviour is also noted in [8] for the case of large damping in the WaveBob PTO system.
  For the closed OWC, the closed orifice equates to infinite turbine damping.

4.2 | Regular waves

The analysis of the regular waves induced motion begins in Section 4.2.1, by examining the input waves used for the experiments. Next, the resulting time series of body displacements are presented in Section 4.2.2. Due to a large number of tests (27 different frequencies), only a subsection of the results can be shown. However, the important information is condensed into a form which can be easily displayed and interpreted, through the maximum displacement at each frequency (Section 4.2.3) and a frequency domain analysis (Section 4.2.4).

4.2.1 | Wave generation

Although a target wave amplitude of 0.01 m was set, the wavemaker does not perform equally well at all frequencies. For example, Figure 9(a,b) plot the measured FSE for the 0.4 and 1 Hz waves, respectively, showing the amplitude at 0.4 Hz more than doubles that at 1 Hz. The actual wave amplitude generated at each frequency is therefore measured and plotted in Figure 9(c), so that the results in the subsequent sections can be normalised against these values. The amplitude is calculated by taking the average of the maximum and minimum FSE between each zero crossing, using the last quarter of the time series.

Most importantly is the wavemaker's ability to reproduce the same wave series on subsequent tests, to ensure the open and closed OWCs are subjected to the same input conditions when comparing their motion response. The repeatability of the wavemaker was tested and confirmed, as demonstrated and discussed in Section 4.3.1.

4.2.2 | Body motion—time series

Figure 10 plots the heave, pitch and roll displacement results for the Open and Closed OWCs. Due to space constraints, only four example frequencies are shown, 0.4, 0.8, 1 and 1.2 Hz. In Figure 10, the large amplitude motion at 0.4 Hz is due to the large amplitude input wave at this frequency (see Figure 9). The amplitude of the pitch motion is additionally influenced by resonance, since 0.4 Hz corresponds to the natural frequency of the pitch DoF. Although the roll natural frequency is also 0.4 Hz, there is no direct wave excitation of the roll DoF for an axisymmetric body, thus the roll motion is much less than the other DoFs.

For the 0.8 Hz frequency wave, parametric pitch and roll motion can be observed in Figure 10, identifiable since the oscillations are at half the frequency of the incident wave in Figure 10. This frequency equals twice the damped natural frequency of the pitch and roll DoFs, thus parametric resonance

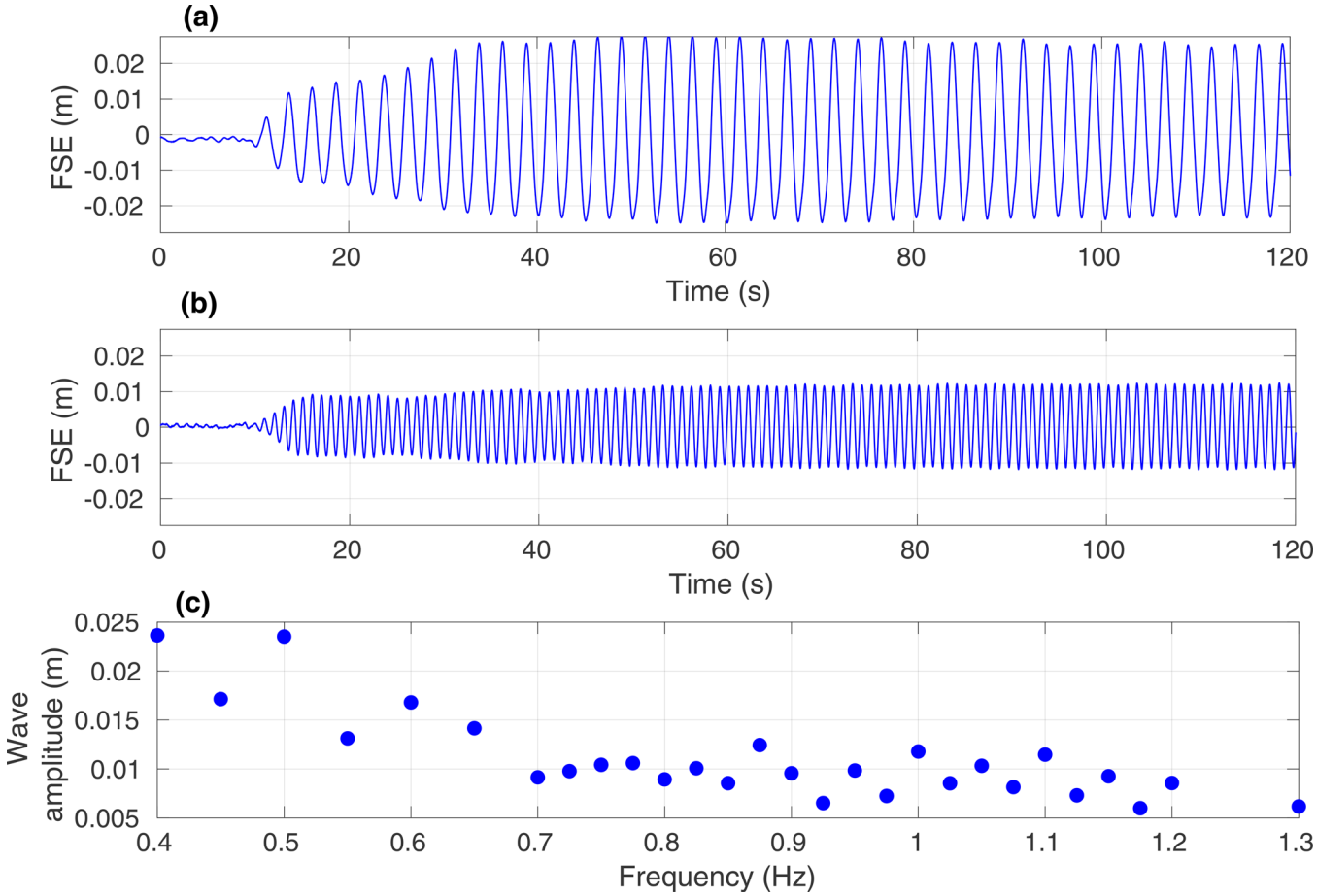

FIGURE 9 Measured FSE for the (a) 0.4 and (b) 1 Hz wave. (c) Average wave amplitude at each frequency tested

is expected if the heave motion exceeds a certain threshold. The parametric motion is observed to transfer energy between the pitch and roll modes. In the case of the 1 Hz frequency wave, parametric resonance can be observed for the Closed OWC but not for the Open OWC. At 1.2 Hz, the heave motion in Figure 10(j) is larger for the Open OWC than for the Closed OWC, which can be expected since the heave natural period for the Open OWC is much closer to 1.2 Hz than the natural period for the Closed OWC (see Table 2). In Figures 10(k, l), it can be seen that no parametric resonance occurs for either the Open or Closed OWCs at 1.2 Hz.

4.2.3 | Body motion—maximum displacement

The maximum displacements per unit wave amplitude are plotted in Figure 11 for each frequency and for three DoFs. Comparing the open and closed OWCs, it can be seen that both exhibit large pitch and roll motions, of similar amplitude, around twice the natural frequency of these DoFs (0.8 Hz). However, for frequencies higher than this, the pitch and roll amplitudes of the closed OWC remain large, and are always bigger than those of the open OWC, which rapidly decrease to non-resonant amplitudes. The pitch amplitude of the open OWC is seen to increase again around the natural heave period, where the heave amplitudes are observed to be large (see Section 2 for the relationship between increased heave amplitude and increased frequency range for the occurrence of parametric resonance).

These experimental results provide some confirmation to the investigated hypothesis that the amount of parametric resonance should be reduced for the open OWC, due to the decoupling of the Spar Buoy and water column motion when the air chamber is open, analogous to the way the notch filter decouples the motion of the two bodies in the WaveBob [8] (see Section 1.2). However, another contributing factor to the reduced parametric resonance might be due to the increased heave natural frequency of the open OWC compared to the closed OWC. The heave natural frequency for the closed OWC is about 0.28Hz greater than the pitch and roll natural frequencies. Whereas, for the open OWC, the heave natural frequency is 0.36Hz greater than the pitch and roll natural frequencies. Therefore, the heave response of the open OWC will be less than that of the closed OWC for frequencies near the pitch/roll parametric frequency. Thus, the occurrence of parametric resonance should be less for the open OWC than for the closed OWC in this frequency band.

To better understand how much of the reduced parametric resonance in the open OWC is due to the decoupling of the

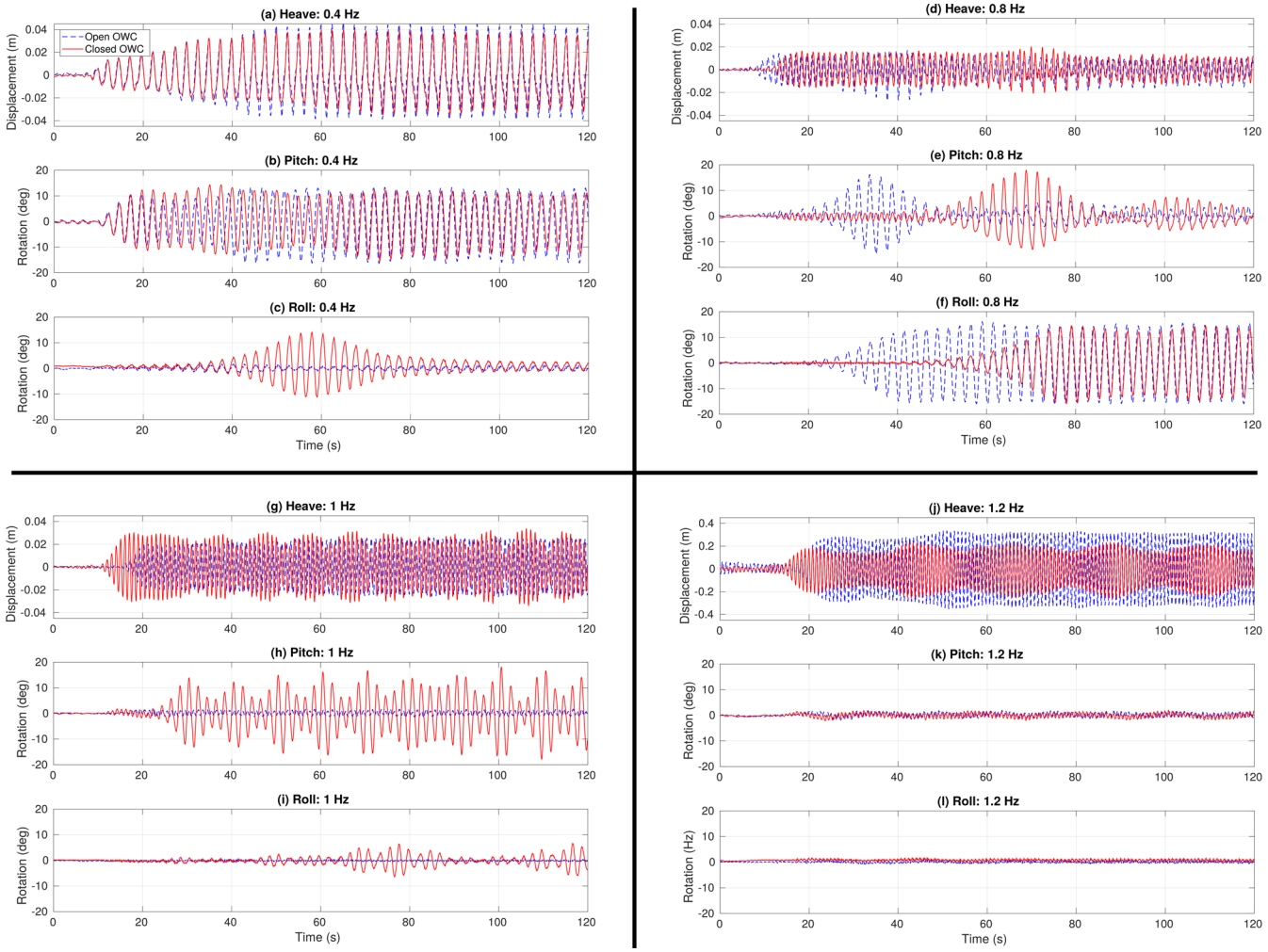

FIGURE 10 (a, d, g, j) The measured heave, (b, e, h, k) pitch and (c, f, i, l) roll displacements for three different wave frequencies.

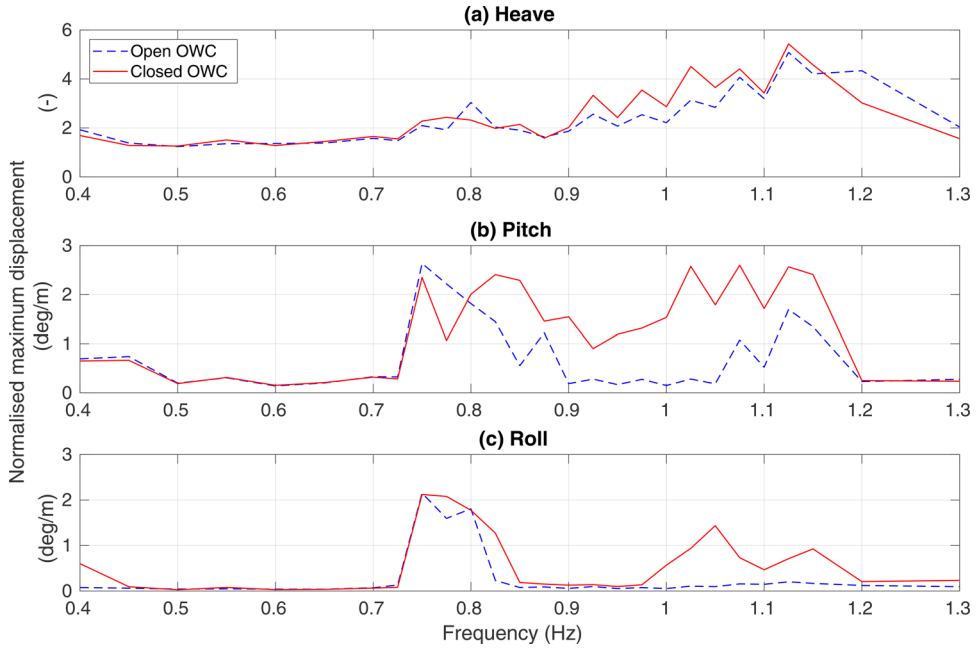

FIGURE 11 The maximum displacement per unit wave amplitude for heave, pitch and roll, as a function of the frequency

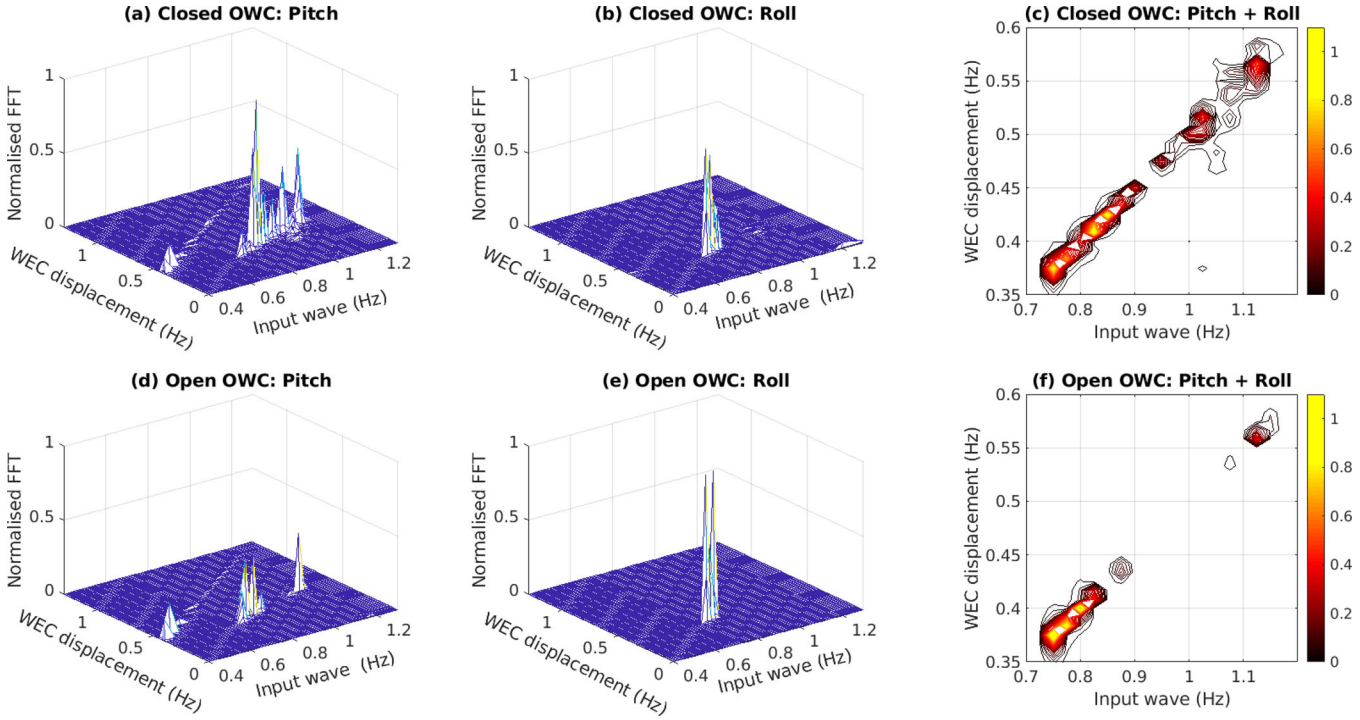

FIGURE 12 The frequency domain results for the (a–c) open and (d–f) closed OWCs. The FFT of the (wave amplitude normalised) pitch time series, for each of the tested input wave frequencies, are shown in (a) and (d). Similarly, the results for roll are shown in (b) and (e). To simplify the comparison, the FFT values in these plots are normalised by the largest value in the four plots. The sum of the pitch and roll normalised FFT values are shown in (c) and (f), zoomed in on the frequency ranges corresponding to parametric resonance.

Spar Buoy and water column motion and how much is due to the increased heave natural frequency, future tests should incorporate a wave gauge inside the OWC Spar Buoy to measure the motion of the water column. Analysing the relative motion of the Spar Buoy and the water column for both the open OWC and closed OWC tests, can provide information on the decoupling effect produced by opening the top of the air chamber.

Figure 11 also shows that the occurrence of parametric resonance is more prevalent in pitch than in roll. The design of the moorings make the system non-axisymmetric, resulting in different natural frequencies and damping values for the pitch and roll DoFs. The natural frequency of roll is about 2.5% lower than pitch, thus the roll DoF is slightly less prone to parametric resonance for higher frequencies. There is more damping in roll than in pitch due to the non-axisymmetric moorings. The roll damping measured in the previous experiments [16] is about 65% larger than the measured pitch damping. As shown in Figure 5 increased damping decreases the parametric resonance region, thus roll is less susceptible to parametric resonance than pitch.

4.2.4 | Body motion—frequency domain

While the maximum displacements provide a decent metric to judge the ability of the open OWC to influence the prevalence of parametric resonance (compared to the closed OWC), performing an FFT on the time series and observing the location and amplitude of the spectral peaks offer two additional insights:

- **Location**—The key signature of parametric resonance is a period-doubling compared to the input oscillations.
  This can be manually observed and verified in Figures 10(e,f,h,i).
  However, in the frequency domain, the location of the peaks give an automatic verification whether the frequency of the pitch/roll motions is half the input wave frequency.
- **Amplitude**—The amplitude of the frequency response is a measure of the energy in the time domain signal.
  Therefore, for tests with the same time span, the amplitude of the frequency response indicates the relative time duration for which large amplitude motions occur.
  For example, consider the pitch and roll motions, for both the open and closed OWCs, at 0.8 Hz, in Figure 10(e, f).
  The maximum displacement for the four time series is nearly identical.
  However, this maximum amplitude only occurs for one or two periods in pitch, but for over 20 periods in roll, and for much longer in the open OWC than in the closed OWC.

Figure 12 displays the frequency domain information, obtained by performing an FFT on the body motion time series to give the WEC displacement power spectra for each of the 27 different input wave frequencies. The pitch results are plotted in Figure 12(a, d), where the large peaks from

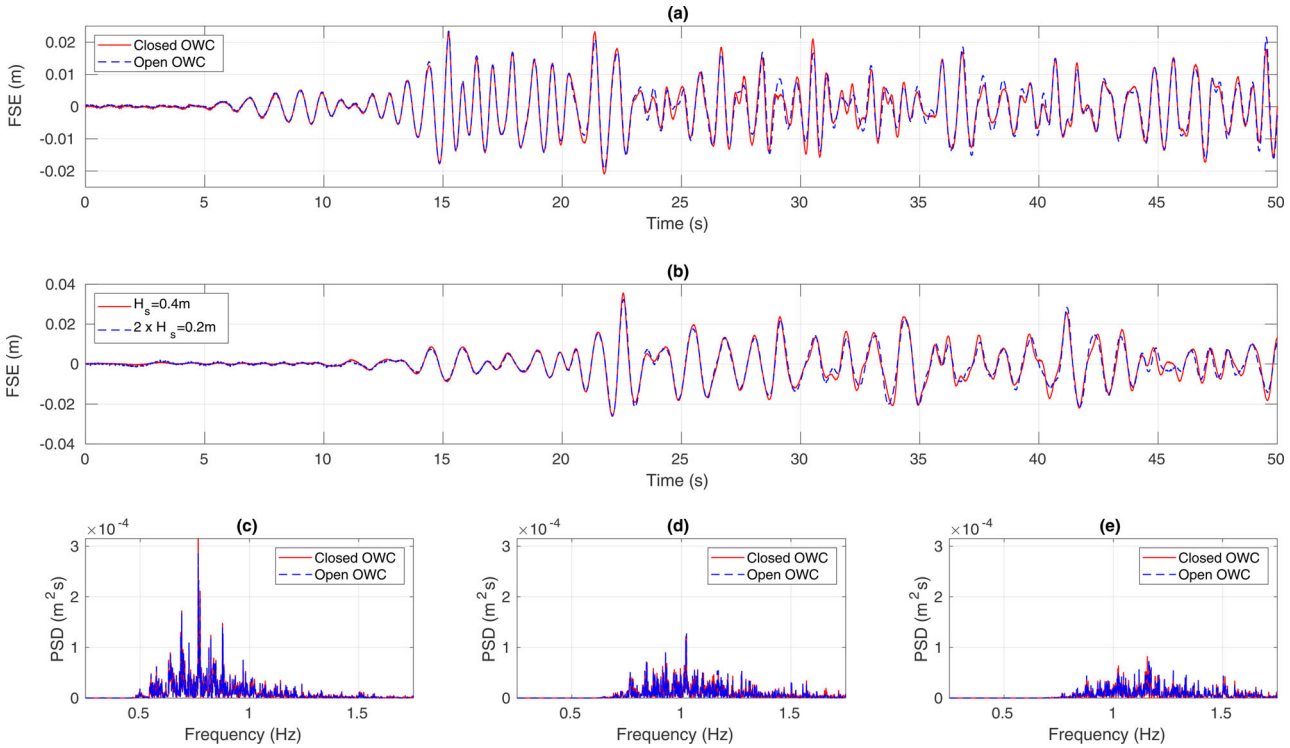

FIGURE 13 (a) Measured FSE during the open and closed WEC experiments for the $H_s = 0.04$ m and $F_p = 1.25$ Hz sea state, (b) measured FSE for the $H_s = 0.04$ m and $F_p = 0.75$ Hz and two times the measured FSE for the $H_s = 0.02$ m and $F_p = 0.75$ Hz sea states during the Closed WEC experiment, (c) the power spectral density (PSD) for the $H_s = 0.04$ m and $F_p = 0.75$ Hz sea state, (d) the PSD for the $H_s = 0.04$ m and $F_p = 1$ Hz sea state, (e) the PSD for the $H_s = 0.04$ m and $F_p = 1.25$ Hz sea state.

parametric resonance can be seen occurring with the WEC displacement frequency being half of the input wave frequency. Also seen in the plot is a second smaller ridge of peaks running diagonally across the plot, where the WEC displacement frequency equals the input wave frequency, corresponding to normal wave-driven motion. This second smaller ridge of peaks does not appear in Figure 12(b, e), since there is no direct wave excitation for the roll DoF in an axisymmetric body. However, large amplitude peaks due to parametric resonance can be seen for the roll motion.

Figure 12(c, f) provide a visual means to best compare the occurrence of parametric resonance in the open and closed OWCs, by displaying a contour plot of the total energy parametrically transferred to pitch and roll. As shown in Figure 10(e, f), the parametric motion can transfer between pitch and roll, so it is important to consider them together when assessing the occurrence of parametric resonance. Comparing plots in Figure 12(c, f), it can be observed that the open OWC is able to reduce the range of frequencies for which parametric resonance occurs.

4.3 | Irregular waves

The analysis of the irregular waves induced motion follows the same format as in Section 4.2 for the regular waves. First the input waves are examined in Section 4.3.1. Next, the resulting time series of body displacements are presented in Section 4.3.2. Then the maximum displacements are examined in Section 4.3.3 followed by a frequency domain analysis in Section 4.3.4.

4.3.1 | Wave generation

As shown in Section 4.2.1, the wavemaker does not generate the exact target wave height and does not perform equally well at all frequencies. Thus, for irregular waves, it is unlikely the wavemaker will exactly generate the target wave signals derived from the JONSWAP spectra (detailed in Section 3.1.3). However, it is not crucial that the exact target wave signal is generated. Instead, the main requirement is that the same wave series is generated for the closed and open OWC experiments, to allow fair comparison between the resulting WEC motions.

Due to the long duration of the irregular waves experiments (900 s) and because knowledge of the exact input wave signal is not vital for the analysis, separate "wave only" experiments, without the WEC in the tank, were not performed prior to the irregular wave-induced motion tests. Alternatively, the FSE elevation is measured during the actual experiments with the WEC in the tank. Figure 13(a) is a plot of the first 50 s of the FSE measured by a wave probe located 1.2 m upwave of the WEC (see Figure 6), for both the closed and open OWC experiments, considering an input wave series with $H_s = 0.04$ m and a $F_p = 1.25$ Hz. The graph confirms the ability of the wavemaker

to produce the same wave series for repeated experiments, with the measured FSE for the closed and open OWC experiments being virtually identical for the first 23 s. In the second half of the graph, some minor differences can be observed between the two signals, which can be attributed to waves radiated and/or diffracted from the WEC, which has a different resulting motion for the closed and open OWC cases.

In total, 12 different wave spectra were tested, with three different peak frequencies and four different significant wave heights. To investigate the effect that the significant wave height has on the occurrence of parametric resonance, the same random phase shifts were applied to each frequency component in all of the spectra, resulting in the set of four input wave signals at a given peak frequency value being identical scaled versions of each other. Therefore, the measured FSE should also be identical scaled versions for each of the different significant wave heights at a given peak frequency, so long as the nonlinear wave interaction is negligible and the linear supposition holds for the sum of the wave components with different frequencies within the spectrum. This is demonstrated in Figure 13(b), which compares the measured FSE for the $H_s = 0.04$ m and $F_p = 0.75$ Hz against double the measured FSE values for the $H_s = 0.02$ m and $F_p = 0.75$ Hz sea states during the closed WEC experiment, showing close agreement between the two measurements.

The ability to investigate the effect that the peak frequency has on the occurrence of parametric resonance was hindered by the performance of the wavemaker. Ideally, the response of the system, as a function of the wave frequency, should be obtained by maintaining a constant wave height. However, the wavemaker does not perform equally well at all frequencies. The difference between the target and generated significant wave heights was thus frequency-dependent. This is displayed in Figure 13(c, d), which show the power spectral density (PSD) plots for the irregular waves with H_s=0.04m at F_p=0.75, 1 and 1.25 Hz, respectively. The amplitude for the PSD is seen to be largest for the 0.75 Hz and then decreases with increasing peak frequency. To quantify the differences between the target and the generated values, the significant wave height is calculated from the measured FSE using the definition [27]:

$$H_s = 4\left(\int_0^\infty S(f)\,\mathrm{d}f\right)^{1/2}, \tag{6}$$

where $S(f)$ is the spectral density function of the measured FSE. The significant wave height measured values are listed in Table 3 from which it can be seen that the measured significant wave height is lower than the target for all of the generated sea states and that the error increases as the peak frequency increases.

4.3.2 | Body motion—time series

The time series of the heave, pitch and roll displacements, for the open and closed OWCs, are plotted in Figure 14. Due to space constraints, only four example sea states are shown: (1) $H_s = 0.01$ m, $F_p = 0.75$ Hz, (2) $H_s = 0.01$ m, $F_p = 1.25$ Hz, (3) $H_s = 0.04$ m, $F_p = 0.75$ Hz, and (4) $H_s = 0.04$ m, $F_p = 1.25$ Hz. Comparing the results between the $H_s = 0.01$ m and $H_s = 0.04$ m sea states, at a given peak frequency, reveals that as H_s increases by a factor of four the heave motion also increases approximately by the same factor. Contrastingly, for the pitch and roll motions, when H_s increases by a factor of four the parametric resonance is triggered and the motion increases by an order of magnitude.

TABLE 3 Measured significant wave height as a function of the sea state peak frequency, F_p and target significant wave height H_s

H_s \ F_p	0.75 Hz	1.00 Hz	1.25 Hz
0.01 m	0.0089 m	0.0082 m	0.0075 m
0.02 m	0.0186 m	0.0173 m	0.0161 m
0.03 m	0.0286 m	0.0253 m	0.0239 m
0.04 m	0.0386 m	0.0346 m	0.0313 m

The results also demonstrate that the motion amplitudes for pitch and roll are smaller for the open OWC in comparison with the closed OWCs, especially in the case of the roll motion. A quantitative comparison between the rotational motions of the open and closed OWCs for all 12 irregular incident waves is presented in the next subsection.

4.3.3 | Body motion—maximum displacement

The maximum pitch and roll displacements for the open and closed OWCs are plotted in Figure 15(a, b), respectively. From this figure, it can easily be seen that overall the maximum displacement for the open OWC is much smaller than the closed OWC. The only cases where the maximum displacement of the open OWC is larger than the closed OWC is for pitch motion in the $H_s = 0.01$ m sea states with peak frequencies of 1.00 and 1.25 Hz. Yet, once the significant wave height of the sea state increases to $H_s = 0.02$ m, the maximum pitch displacement of the closed OWC is approximately double the maximum pitch displacement of the open OWC for $F_p = 1.25$ Hz, and more than two and half times greater for $F_p = 1.00$ Hz.

In Figure 16 the maximum pitch and roll displacements are normalised against the corresponding measured significant wave heights from Table 3. Without the occurrence of parametric resonance, the normalised results in Figure 16 should be constant if the system is linear. However, due to the nonlinear effects of viscous damping, it is expected that the normalised results should decrease with increasing wave height [28, 29]. This effect can be observed for the roll motion in the sea states with small significant wave heights and for the pitch motion of the open OWC for the $F_p = 1.00$ Hz sea states between $H_s = 0.01$ m and $H_s = 0.02$ m. The nonlinear increase in the pitch and/or roll motion amplitudes due to parametric resonance can be observed by the increase in the normalised results with respect to the significant wave height.

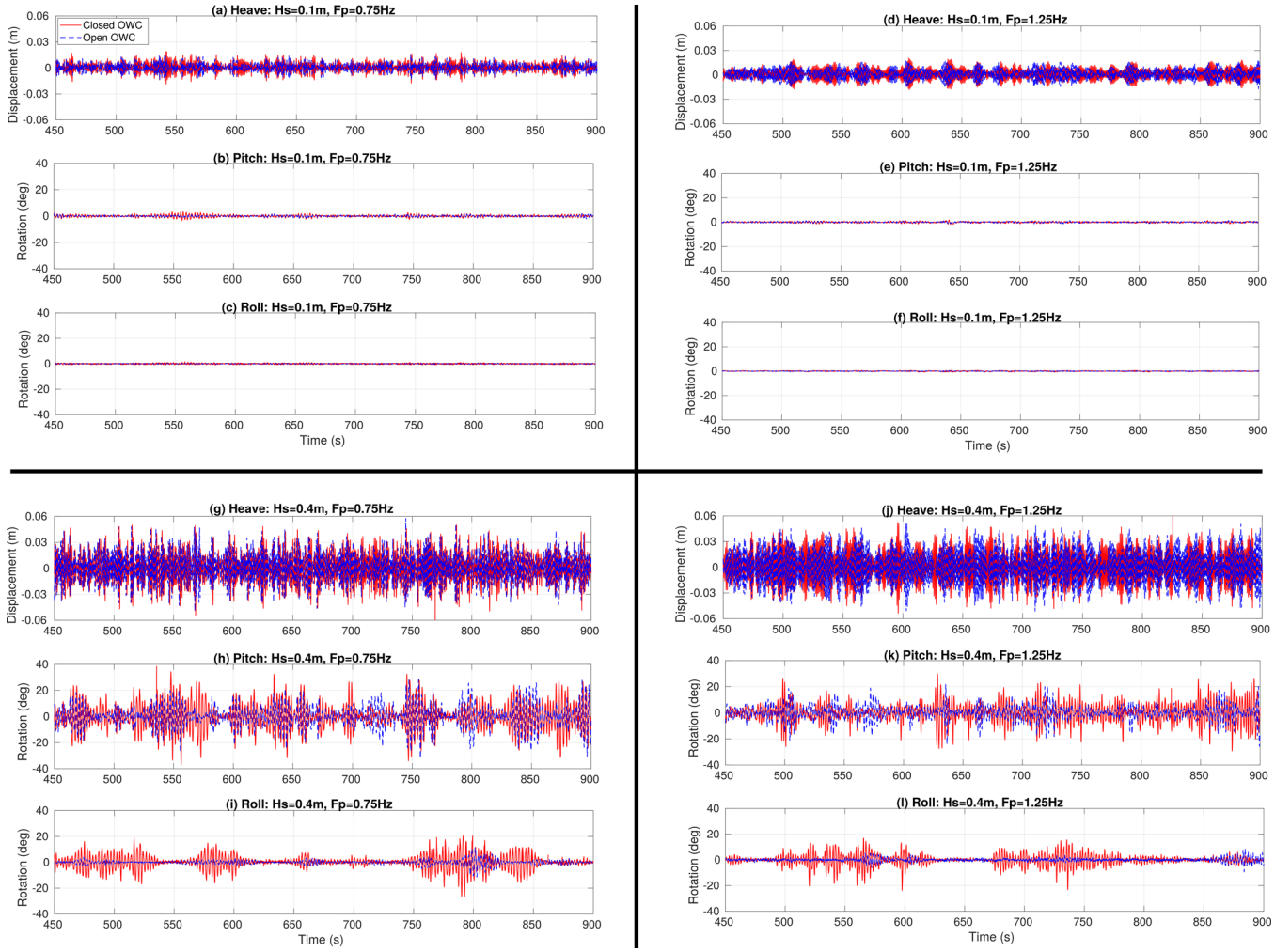

FIGURE 14 The heave, pitch and roll displacements for the (a–c) $H_s = 0.01$ m, $F_p = 0.75$ Hz, (d–f) $H_s = 0.01$ m, $F_p = 1.25$ Hz, (g–i) $H_s = 0.04$ m, $F_p = 0.75$ Hz and (j–l) $H_s = 0.04$ m, $F_p = 1.25$ Hz sea states, respectively

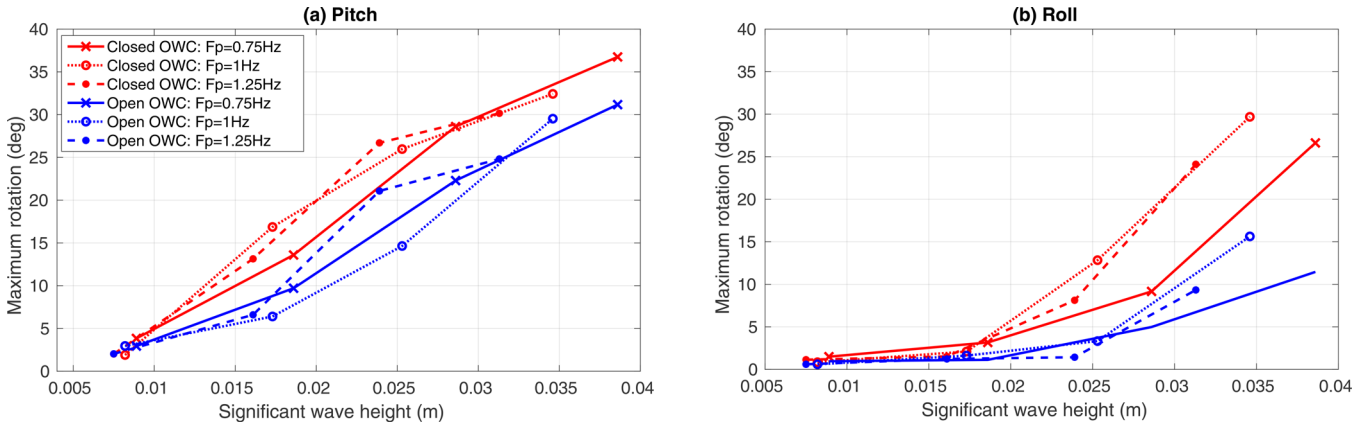

FIGURE 15 Maximum (a) pitch and (b) roll motion for the open and closed OWCs for each peak frequency, as a function on the measured significant wave height

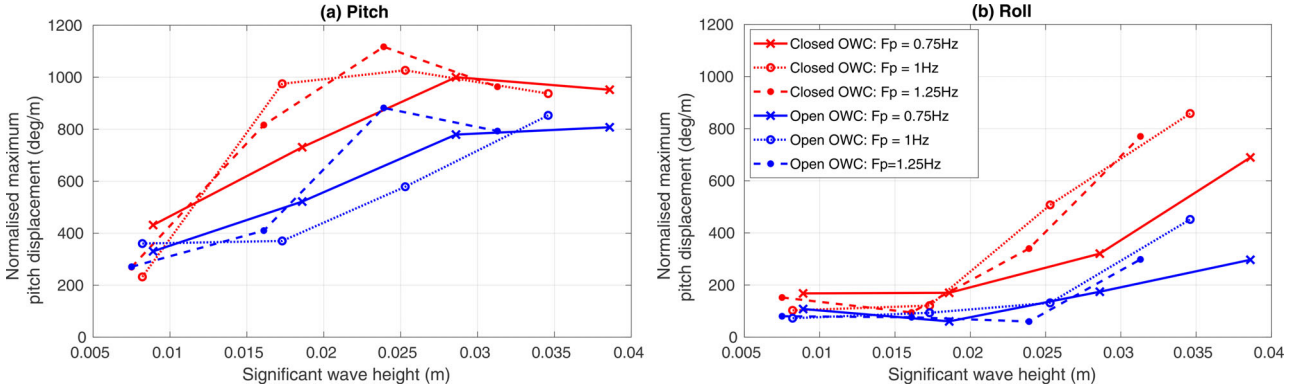

FIGURE 16 Normalised maximum (a) pitch and (b) roll motion for the open and closed OWCs, normalised against the measured significant wave height, for each peak frequency, as a function on the measured significant wave height

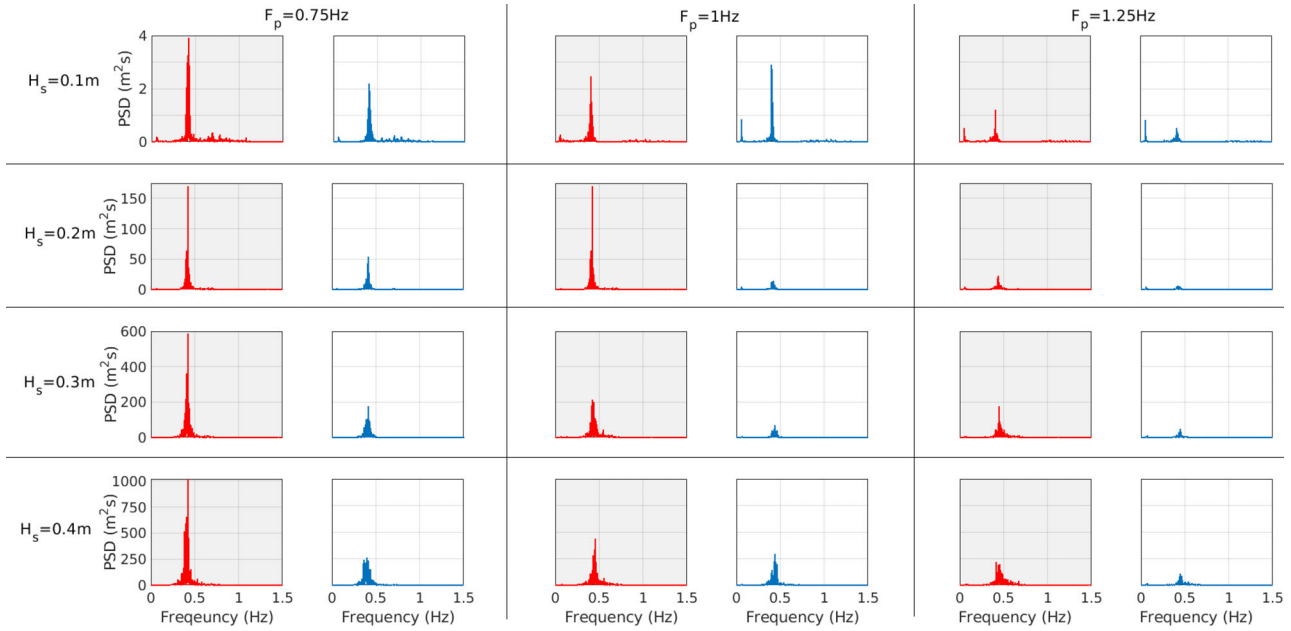

FIGURE 17 The power spectral density (PSD) for the pitch displacement. Results for the closed OWC are plotted in red on the grey graphs and the results of the open OWC are plotted in blue on the white graphs

Results also show that for several sea states the parametric resonance occurs for the closed OWC but does not appear for the open OWC.

4.3.4 | Body motion—frequency domain

As discussed in Section 4.2.4, comparing the results in the frequency domain encapsulates the duration, as well as the amplitude, of the large pitch/roll motions and therefore provides a measure of the total energy. Figures 17 and 18 plot the PSD for the pitch and roll displacements, respectively, for each of the experiments. The results for the closed OWC are plotted in red on the grey graphs and the results of the open OWC are plotted in blue on the adjacent white graphs. A visual comparison of the results for the closed and open OWC configurations at each sea state shows a clear trend that the Open OWC has less motion amplitudes than the closed OWC. The $H_s = 0.01$ m, $F_p = 1.00$ Hz is the only sea state where the open OWC has a larger peak PSD value than the closed OWC. A quantitative comparison is given by calculating the integral under the PSD curves to give the total energy, plotted in Figures 19, which confirms the ability of the open OWC to significantly reduce the motion in the pitch and roll DoFs.

5 | CONCLUSION

The present research studied the parametric resonance behaviour of two OWC spar buoy configurations: closed-air chamber and an open-air chamber. The purpose was to assess the possibility of applying an active control method to a pressure relief valve installed in parallel with the power take-off system to reduce large pitch and roll motions due to parametric resonance.

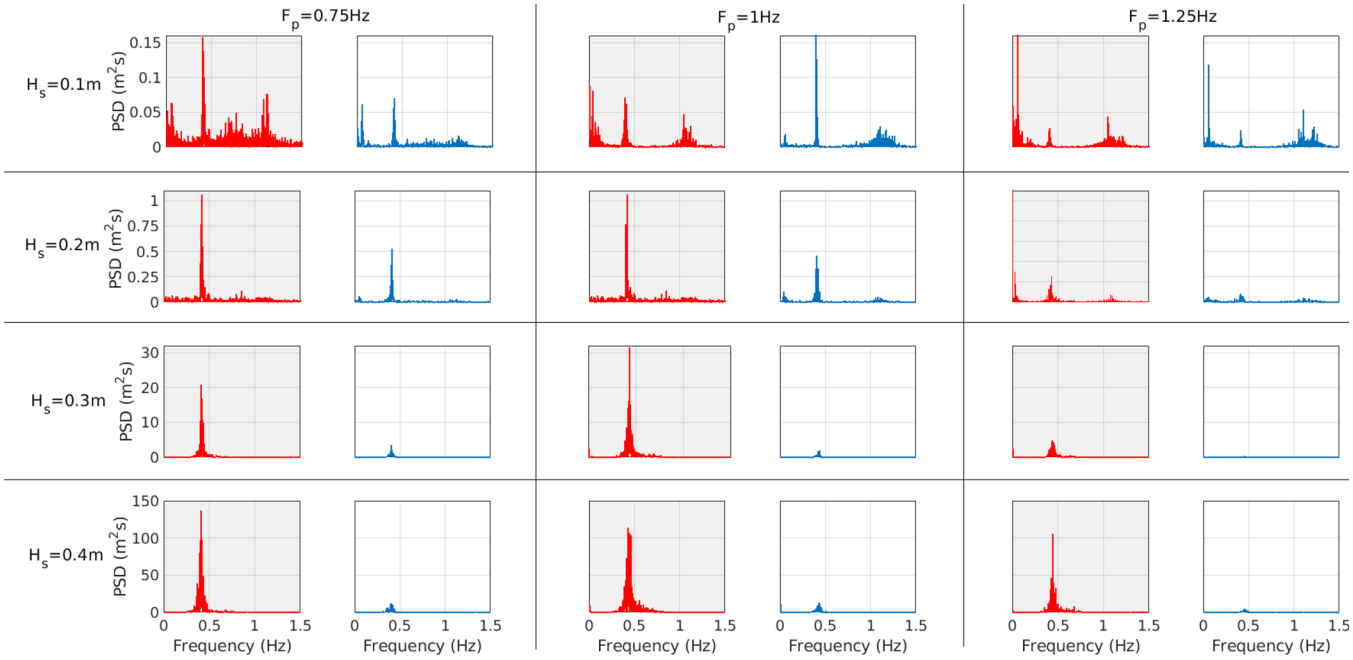

FIGURE 18 The power spectral density (PSD) for the roll displacement. Results for the closed OWC are plotted in red on the grey graphs and the results of the open OWC are plotted in blue on the white graphs

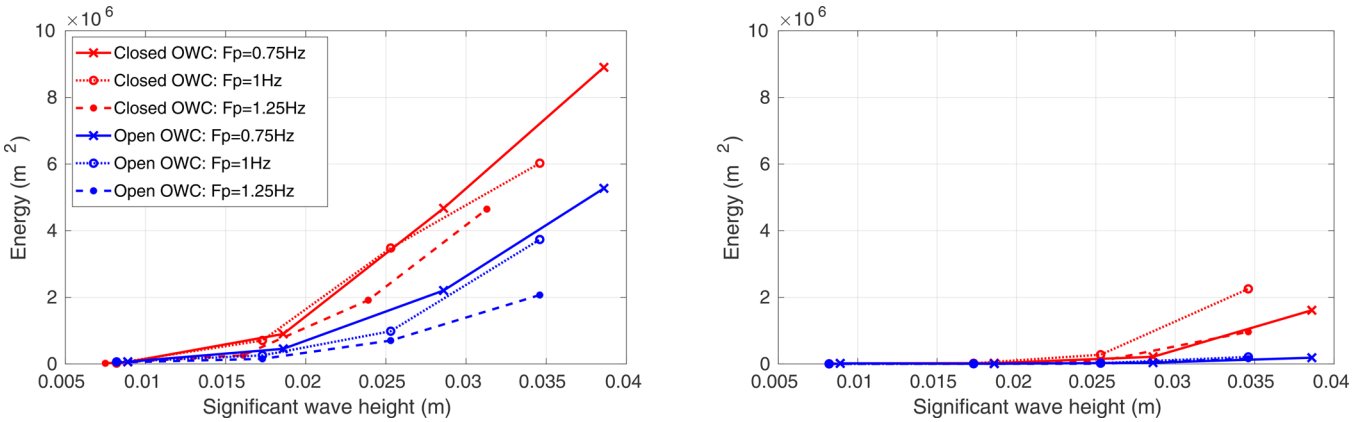

FIGURE 19 Total energy in the (a) pitch and (b) roll DoFs, for each of the irregular input wave experiments

Such relief valve systems have previously been incorporated into OWCs as a mechanism to spill energy and prevent over operating the turbine in extreme conditions [30]. The present study explores a dual purpose for these relief valves, to mitigate the occurrence of parametric resonance, since opening a relief valve reduces the coupling between the spar buoy and inner water column, altering the device motion and providing a means to detune the resonant dynamics.

The decay test results proved that opening the air chamber shifts the heave damped natural frequency further away from the frequency region where parametric pitch and roll motions were observed. As expected, the roll and pitch damped natural frequencies for the open and closed air chambers are identical. For certain regular wave frequencies parametric resonance was detected with the air chamber closed but not spotted with the air chamber open. With irregular waves, the results showed that when parametric resonance was detected, the pitch and roll motion amplitudes were lower with the open-air chamber than with the closed-air chamber. The results also revealed that the time duration of parametric resonance is shorter for the open air chamber than for the closed air chamber.

The reported results opened the possibility of detuning the frequency coupling by switching between the two configurations whenever parametric resonance is detected. This switching may be implemented through the operation of an air pressure relief valve installed in parallel with the PTO system, as an active control method to counteract the development of parametric

resonance. A relief valve was not considered in this experimental campaign. The complexity of designing, building and controlling in real-time a small-scale relief valve installed in a buoy model was beyond the scope of this work. Future research will focus on the design and control of a relief valve in a small scale experimental setup of an OWC spar buoy.

ACKNOWLEDGEMENTS

This project has received funding from the European Union's Horizon 2020 research and innovation programme under the Marie Sklodowska-Curie grant agreement No 867453. The IST Team was partially funded by the Portuguese Foundation for Science and Technology (FCT), through IDMEC, under LAETA project UID/EMS/50022/2020.

ORCID

Josh Davidson https://orcid.org/0000-0001-5966-4272
João C. C. Henriques https://orcid.org/0000-0001-5850-9641

REFERENCES

1. Koo, B.J., et al.: Mathieu instability of a spar platform with mooring and risers, Ocean Eng. 31, 17, 2175–2208 (2004)
2. Rho, J.B., et al.: A study on Mathieu-type instability of conventional spar platform in regular waves, Int. J. of Offshore and Polar Eng. 15(02) (2005)
3. Neves, M.A.S., et al.: On the occurrence of Mathieu instabilities of vertical cylinders. In: Proc. ASME 27th International Conference on Offshore Mechanics and Arctic Engineering pp. 619–627. ASME, New York (2008)
4. Jang, H., Kim, M.: Mathieu instability of Arctic Spar by nonlinear time-domain simulations, Ocean Eng. 176, 31–45 (2019)
5. Fossen, T., Nijmeijer, H.: Parametric Resonance in Dynamical Systems. Springer, Berlin, Heidelberg (2011)
6. Davidson, J., et al.: Nonlinear rock and roll–Modelling and control of parametric resonances in wave energy devices. In: Proc. 9th Vienna Int. Conf. Math. Modelling, pp. 21–22. Maynooth University, Maynooth (2018)
7. Davidson, J., Costello, R.: Efficient nonlinear hydrodynamic models for wave energy converter design - A scoping study, J. of Mar. Sci. and Eng. 8(1), 35 (2020) https://www.mdpi.com/2077-1312/8/1/35
8. Villegas, C., van der Schaaf, H.: Implementation of a pitch stability control for a wave energy converter. Proc. 10th European Wave and Tidal Energy Conference, University of Southampton, Southampton (2011)
9. Beatty, S.J., et al.: Experimental and numerical simulations of moored self-reacting point absorber wave energy converters. In: Proc. 25th International Ocean and Polar Engineering Conference, pp. 1–11. ISOPE, Cupertino, CA (2015)
10. Kurniawan, A., et al.: Numerical modelling and wave tank testing of a self-reacting two-body wave energy device. In: Ships and Offshore Structures, pp. 1–13. Taylor and Francis, Oxfordshire (2019)
11. Tarrant, K. and Meskell, C.: Investigation on parametrically excited motions of point absorbers in regular waves, Ocean Eng. 111, 67–81 (2016)
12. Giorgi, G., Ringwood, J.V.: Articulating parametric resonance for an owc spar buoy in regular and irregular waves, J. Ocean Eng. and Mar. Energy 4, (4), 311–322 (2018)
13. Gomes, R.P.F., et al.: Testing of a small-scale floating OWC model in a wave flume. In: International Conference on Ocean Energy pp. 1–7. University of Plymouth, Plymouth (2012)
14. Gomes, R.P.F., et al.: Wave channel tests of a slack-moored floating oscillating water column in regular waves. In: Proc. 11th European Wave and Tidal Energy Conference, pp. 6–11. (2015)
15. Gomes, R.P.F., et al.: Time-domain simulation of a slack-moored floating oscillating water column and validation with physical model tests, Renewable Energy 149, 165–180 (2020)
16. Gomes, R.P.F., et al.: An experimental study on the reduction of the dynamic instability in the oscillating water column spar buoy. In: Proc. 12th European Wave and Tidal Energy Conference, pp. 1105-1–1105-10. University of Plymouth, Plymouth (2017)
17. Gomes, R.P.F., et al.: Experimental tests of a 1: 16th-scale model of the spar-buoy OWC in a large scale wave flume in regular waves. In: Proc. ASME 37th International Conference on Ocean, Offshore and Arctic Engineering, pp. 1–10. ASME, New York (2018)
18. Giorgi, G., et. al.,: The effect of mooring line parameters in inducing parametric resonance on the spar-buoy oscillating water column wave energy converter. Journal of Marine Science and Engineering 8(1), 29 (2020)
19. Gomes, R.P.F., et al.: An upgraded model for the design of spar-type floating oscillating water column devices. Proc. 13th European Wave and Tidal Energy Conference, Napoli, Rome, 1–6 Sept (2019)
20. Sheng, W., et al.: Experimental studies of a floating cylindrical OWC WEC . Proc. ASME 31st International Conference on Ocean, Offshore and Arctic Engineering, pp. 169–178. ASME, New York, NY (2012)
21. Payne, G.S., et al.: Assessment of boundary-element method for modelling a free-floating sloped wave energy device. Part 2: Experimental validation. Ocean Eng. 35(3–4), 342–357 (2008)
22. Haslum, H.A., Faltinsen, O.M.: Alternative shape of spar platforms for use in hostile areas. Paper presented at Proc. Offshore Technology Conference Houston, TX, 3–9 May 1999
23. Den Hartog, J.P.: Mechanical Vibrations. Third Edition, McGraw-Hill, New York (1947)
24. Biran, A., López Pulido, R.: Ship Hydrostatics and Stability. Second Edition, Butterworth-Heinemann, Oxford (2014)
25. Giorgi, G., et al.: Detecting parametric resonance in a floating oscillating water column device for wave energy conversion: Numerical simulations and validation with physical model tests. Appl. Energy 276, 115421 (2020)
26. Gomes, R.P.F., et al.: Hydrodynamic optimization of an axisymmetric floating oscillating water column for wave energy conversion. Renewable Energy 44, 328–339 (2012)
27. Tucker, M.J., Pitt, E.G.: Waves in ocean engineering. In: Ocean Engineering, Elsevier, New York (2001)
28. Yu, Y.H., Li, Y.: Reynolds-Averaged Navier–Stokes simulation of the heave performance of a two-body floating-point absorber wave energy system. Comp. & Fluids 73, 104–114 (2013)
29. Davidson, J., et al.: Linear parametric hydrodynamic models for ocean wave energy converters identified from numerical wave tank experiments, Ocean Eng. 103, 31–39 (2015)
30. Falcão, A.d.O., Justino, P.: OWC wave energy devices with air flow control, Ocean Eng. 26, 12, 1275–1295 (1999)

How to cite this article: Davidson J, Henriques JCC, Gomes RF, Galeazzi R. Opening the air-chamber of an oscillating water column spar buoy wave energy converter to avoid parametric resonance. IET Renew. Power Gener.. 2021;15:3109–3125. https://doi.org/10.1049/rpg2.12204